AIMS Geosciences

AIMS Geosciences, 11(4): 923–945.
DOI: 10.3934/geosci.2025040
Received: 06 March 2025
Revised: 09 September 2025
Accepted: 27 October 2025
Published: 11 November 2025

https://www.aimspress.com/journal/geosciences

Research article

Geotechnical characterization and strain-rate dependent response of peat from the Netherlands

C Zwanenburg[1,*], M Konstadinou[1] and EP Grünewald[2]

[1] Deltares, P.O. box 177, 2600 MH, Delft, The Netherlands
[2] ProRail, P.O. box 2038, 3500 GA, Utrecht, The Netherlands

* **Correspondence:** Email: cor.zwanenburg@deltares.nl; Tel: 0031 651114312.

Abstract: For construction and maintenance of infrastructure, a good understanding of the engineering properties of the subsoil is needed. In some areas, the subsoil contains deposits of peats and organic soils. Although many studies on the strength of peats, in the laboratory and the field, have been published, little is known on the strain-rate dependency of peat strength. In this paper, we discuss a series of triaxial and direct simple shear (DSS) tests conducted at different strain rates. The results were compared to trends observed in clays. Moreover, numerical simulations were conducted using the Creep SClay1 model. Equivalent to clay behaviour, the tested peat showed the impact of rate effects. The higher the shearing rate, the higher the undrained shear strength. The numerical simulations captured the peat behaviour reasonably well. Moreover, heterogeneity of the tested material masked a possible trend with over-consolidation ratio (OCR). The tests provided a clear starting point for further exploring rate effects in testing peats. Additional tests and numerical simulations by different constitutive models that account for viscous effects are suggested to develop an understanding of peat behaviour.

Keywords: mechanical behaviour; organic soil; peat; laboratory testing; rate effects

1. Introduction

Peat is a complex foundation material (among others [1,2]); yet, when building in areas with considerable peat deposits, its complexity has to be dealt with. Over the years, several researchers have studied the strength properties of peats, in which the presence of fibres plays an important role [2–7]. Interestingly, these authors report strength characteristics for peats that are higher than typically observed for non-organic soils.

Different correlations in which the strength characteristics for peats are related to water content, loss on ignition, or density are discussed by the researchers in [8] and [9]. These correlations support the above-mentioned tendency by showing high strength characteristics for a high organic content level.

Several field trials, in which an embankment or shallow foundation was loaded to failure, showed the applicability of conventional field and laboratory testing for parameter assessment for peats [10–13]. The different field trials showed that the mobilised high strength for peats, or organic soils in general, follows with large deformation. This results in the development of rupture planes [11] or failure at the interface of the peat deposit and underlaying clay layers, [12].

Despite the studies on peat strength mentioned above, little is known on the strain rate dependency of peat strength. For instance, the researchers in [14] and [15] link the strain rate dependency observed for clays to the isotach framework for viscous behaviour [16,17]. In this paper, we discuss a series of triaxial and direct simple shear (DSS) tests on peat, which include a variation in applied shear strain rate and tests if the trends found for clays are also found when testing peats. Moreover, the constitutive model Creep-SClay1, proposed by the researchers in [15], is used to simulate the data.

In Section 2, we discuss the background of rate effects in undrained shearing for clays. In Section 3, we give a description of the test site where the tested material was sampled. In Section 4, we give the testing plan. In Section 5, we further specify the tested material, and Sections 6 and 7 show the test results. In Section 8, we provide the results of numerical simulations, while the discussion of the results are provided in Section 9. In Section 10, we finalise with conclusions.

2. Rate effects in undrained shearing

Rate effects in the undrained shear strength, s_u, of clays is well established. Among others, Casagrande & Wilson [18] describe the strain rate dependency of different clays and shales and relate the results to failures along the Panama canal. Additionally, researchers explore the rate effects on shear strength by triaxial testing [19–22]. These studies show a logarithmic relation between the undrained shear strength and the applied loading rate. The impact of the loading rate on the undrained shear strength is captured by parameter ρ_q:

$$\rho_q = \frac{\Delta\left(q_f \middle/ \sigma'_0\right)}{\Delta \log\left(\frac{d\varepsilon_a}{dt}\right)} \tag{1}$$

Here:

q_f = the deviatoric stress at failure, $q_f = 2 \times s_u$, in which s_u represents the undrained shear strength;

σ'_0 = isotropic consolidation stress;

$\frac{d\varepsilon_a}{dt}$ = applied strain rate, in which ε_a represents the axial strain.

The importance of rate effects in field testing was established by Bjerrum, [23], resulting in a field vane correction factor accounting for differences in rate effects between field testing and embankment failure.

Lunne at al. [24] described rate effects in CPTu testing, which is confirmed by others for T-bar and ball penetrometer testing [25]. Again, a logarithmic relation is found between the undrained shear strength and loading. However, in the field, partly drained or even fully drained behaviour is found for low loading rates in permeable soils. When reaching drained conditions, an increase in strength is found for further reducing the loading rate. This results in a back-bone curve with relatively high undrained strength for high loading rates and high drained strength for low loading rates. A minimum strength is found at the transition between drained and undrained behaviour.

These studies show two different sources for the impact of the loading rate on strength of soils:

1. The transition from drained to partially drained to fully undrained behaviour when the loading rate increases.
2. Viscous effects for fully undrained conditions.

A more in-depth analysis of the second source is provided in [26] for sands and [27], [14] for clays, and [28] for unsaturated soils. These authors relate the viscous effects in undrained shear strength to the isotach principle used in settlement analysis [17,29]. This behaviour is captured in constitutive modelling by the researchers in [15].

In contrast to clays, little is known on the strain rate dependency of the undrained shear strength for peats. However, since peats are sensitive for creep and the rate effects for clays are linked to creep [14], a strong effect is to be expected. Here, we discuss a series of triaxial and DSS tests in which a constant strain rate, different for the different tests, is applied.

3. Test site Zegveld

The test site, Zegveld, is in the western part of the Netherlands (see Figure 1). The test site is owned by the knowledge transfer centre, KTC Zegveld, which is a knowledge centre for agriculture [30]. Besides agricultural studies, the KTC fields are also used for land subsidence studies, with continuous measurement series on land subsidence from 1970, [31].

Due to the available background information on the peat and the easy access to the terrain, peat samples from the Zegveld test site are also used to study engineering properties of peat [32] and others.

The ground level at the test site is at around NAP—2.66 m, [33], with NAP being the Dutch national reference elevation datum, representing approximately mean sea level. The top 0–0.3 m layer contains an organic content, which varies between 50 and 70% of the soil mass. It gradually increases to 80–85% at 0.8 m depth [34]. Wood remnants are common in the top 3 m, while below that, depth sedge and reed dominates the peat constituents [31]. The ground water table is carefully monitored over the years and controlled by the free water in the ditches. The ground water table is maintained at 0.25 m below ground level [31]. Appendix A from [1] provides a classification system

that includes the different aspects of peat. Application of this classification system for the peat found at Zegveld gives:

- The humification is expressed by the Von Post classification, which includes a scale ranging from H_1 for fresh peat to H_{10} for completely humified peat (see [1]). On this scale, the tested samples are moderate humified, H_5–H_6.
- The water content, w, is discussed in Section 5. The reported w = 600% results, following the Hobbs classification, in B_3.
- The fibrosity is assessed visually on a scale 0 to 3 according to [1,35,36]. The presence of fine fibres is scaled as 1 to 2. In the Hobbs classification system, [1], $F_{1\text{-}2}$.
- The coarse fibres and wood remnants are also categorised in a range of 0–3, resulting R_2 in the coarse fibres and W_2 for wood remnants in the Hobbs classification system.
- The organic content is discussed in Section 5. With the Loss On Ignition (LOI) = 82% follows, in the Hobbs classification system, N_4.
- The tensile strength is judged by pulling peat samples apart [1,35,36], resulting in a low Tensile strength in vertical direction and some tensile strength due to interlocking of the fibres in a horizontal direction, TV_0, TH_1.

This results in the extended classification of the Zegveld peat as: $H_{5\text{-}6}B_3F_{1\text{-}2}R_2W_2N_4TV_0TH_1$.

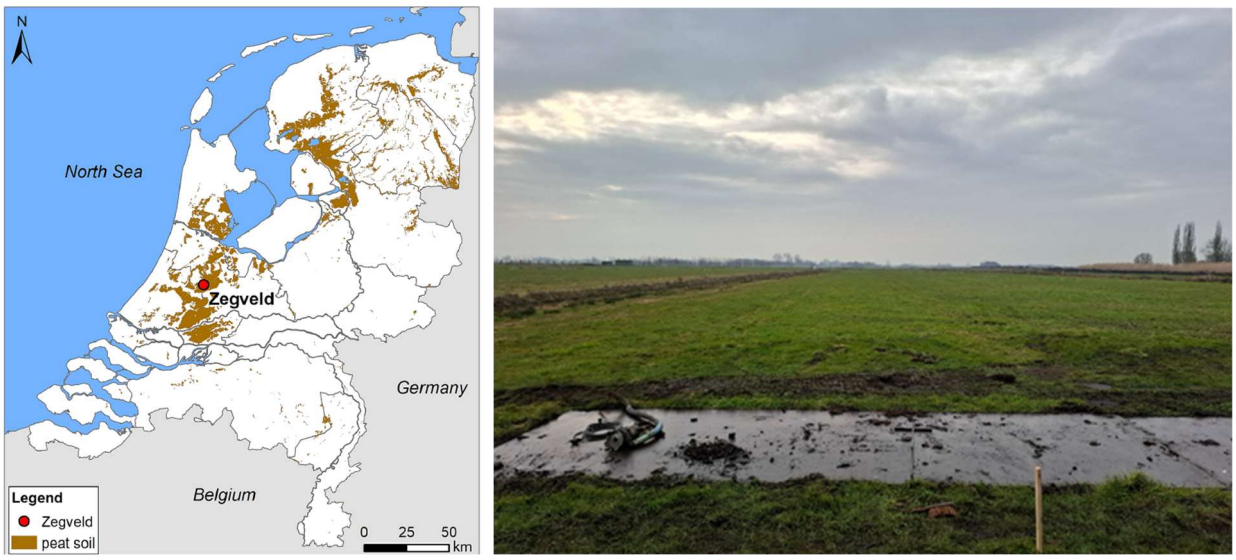

Figure 1. Left: the Zegveld test site (left). Right: the location indicated on the map, from [31], showing the impression of the test site.

Figure 2 shows a CPTu of the test site. The peat deposit has a thickness of approximately 6.2 m and is followed by an 0.8 m thick clay layer and a thick Pleistocene sand deposit.

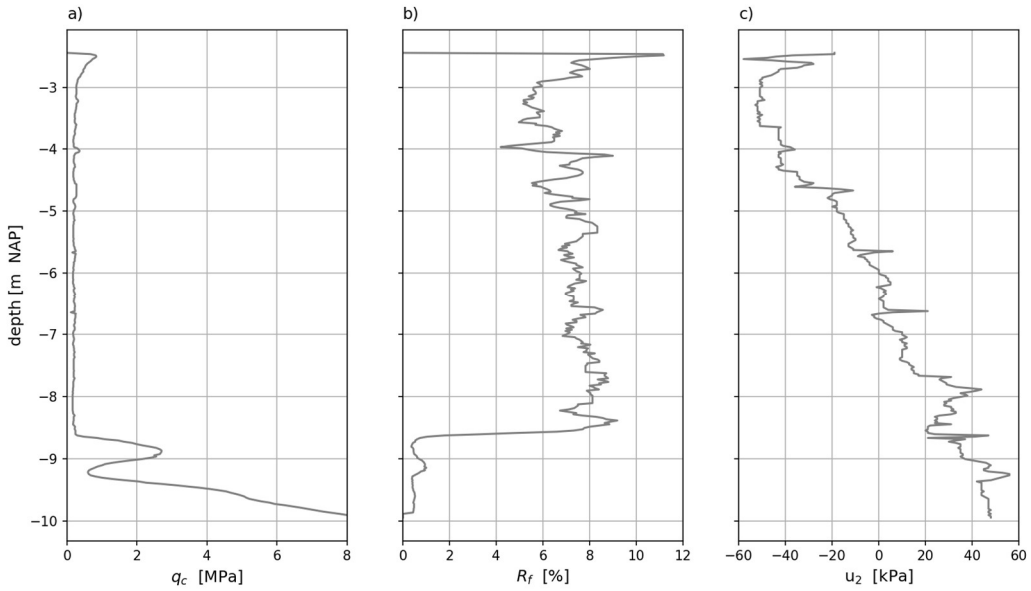

Figure 2. CPTu from the test site. a) Cone resistance q_c, b) Friction ratio, R_f, and c) pore pressure measured at the shoulder of the cone, u_2. Depth related to the reference datum NAP, showing approximate mean sea level.

4. Testing plan

In total, 9 triaxial tests and 6 DSS tests were conducted. Table 1 presents the test specifications. The triaxial test series contained 3 OCR-values combined with 3 different loading rates. The DSS test series combined 2 shearing rates to 2 over-consolidation ratio (OCR)values. Moreover, DSS test series deviated in the application of pre-shearing during consolidation.

The triaxial tests were conducted in a Wille testing machine. The initial diameter size was 67 mm and an initial height 133 mm. The applied load cell had a measurement range 0–1 kN. Paper side drains were used to accelerate consolidation and to improve uniformity of the pore pressure in the specimens during undrained shearing. The measurement frequency was 0.2 Hz, 1 reading per 5 sec, resulting in 181 readings during the shearing phase of the most rapid test. Special care was taken to reduce the friction between the specimen and the top and foot caps by applying silicon grease and an additional membrane between the specimen and the caps.

All specimens were consolidated anisotropically, with the initial ratio of horizontal to vertical effective stress, K_0 from Jacky's formula:

$$K_{0,OC} = K_{0,NC} OCR^{(\sin\varphi')}, \quad K_{0,NC} = 1 - \sin(\varphi') \tag{2}$$

Here:

$K_{0,OC}$; $K_{0,NC}$ = ratio of horizontal to vertical effective stress for over-consolidated, respectively normally consolidated conditions;

OCR = over-consolidation ratio;

φ' = friction angle.

Table 1. Overview of conducted tests.

Test ID	OCR	K_0	σ_{vc}'**	σ_{hc}'**	$d\varepsilon_a/dt$	Δt^*
Triaxial tests	[-]	[-]	[kN/m^2]	[kN/m^2]	[% /hr]	[h]
TX55	1.0	0.35	45	15.8	1	25
TX56	1.0	0.35	45	15.8	10	2.5
TX57	1.0	0.35	45	15.8	100	0.25 (15 min)
TX58	1.5	0.45	30	13.5	1	25
TX59	1.5	0.45	30	13.5	10	2.5
TX60	1.5	0.45	30	13.5	100	0.25 (15 min)
TX76	2.5	0.63	30	18.9	1	25
TX77	2.5	0.63	30	18.9	10	2,5
TX78	2.5	0.63	30	18.9	100	0.25 (15 min)
Test ID	OCR	τ_c***	σ_{vc}'**	σ_{vi}'**	$d\gamma/dt$	Δt^*
DSS tests	[-]	[kN/m^2]	[kN/m^2]	[kN/m^2]	[% /hr]	[h]
DSS66	1.0	10	45	45	5	8
DSS67	1.0	10	45	45	500	0.083 (5 min)
DSS64	1.0	0	45	45	500	0.083 (5 min)
DSS65	4.0	0	120	30	500	0.083 (5 min)
DSS74	4.0	10	120	30	5	8
DSS75	4.0	10	120	30	500	0.083 (5 min)

Note: * duration of the shearing phase, which is ended at an axial strain $\varepsilon_a = 25$ % for triaxial tests and shear strain $\gamma = 40\%$ for DSS tests. ** σ_{vc}' = vertical effective consolidation stress; σ_{hc}' = horizontal effective consolidation stress, and σ_{vi}' = initial effective vertical stress at start shearing phase. *** τ_c = level of pre-shearing; shear stress applied during consolidation.

The applicability of Jacky's formula for peats was established by the researchers in [8]. The friction angle to obtain the K_0—value, given by Table 1, follows from a prior test series on Zegveld peat, resulting in $\varphi' = 45°$.

To prevent large deformation during the consolidation phase, the applied OCR was limited to 2.5, as large deformation might jeopardise the height—diameter ratio at the start of the shearing phase. This ratio should be in the range of 2(H):1(D) [37].

The anisotropic consolidation stress was applied by first rising the cell pressure to its target value followed by applying the vertical plunger load. The over consolidation was reached by reconsolidation at a lower stress condition, which was reached by first reducing the plunger load, followed by reducing the cell pressure. Figure 3 gives the details.

The undrained shear strength was evaluated in terms of peak strength and critical state, *cs* strength, for which the strength at the end of the shearing phase was used as a proxy for the *cs* strength. In analysing the data, a correction was applied for the membrane, and filter paper was applied according to [38].

Additionally to the triaxial testing, 6 DSS tests were conducted. The over consolidated specimens were first consolidated at a consolidation stress of 120 kN/m^2 followed by a re-consolidation at 30 kN/m^2, inducing OCR = 4. All specimens were sheared at constant volume to mimic undrained behaviour [39].

To study the rate effects, the shearing rate varied between the standard shearing rate for peats, 5 %/h and a 100-times faster, 500 %/h. Tests were conducted with and without pre-shearing, in which pre-shearing was believed to be relevant for stress conditions at the toe of an embankment. Pre-shearing was applied under drained, constant stress conditions.

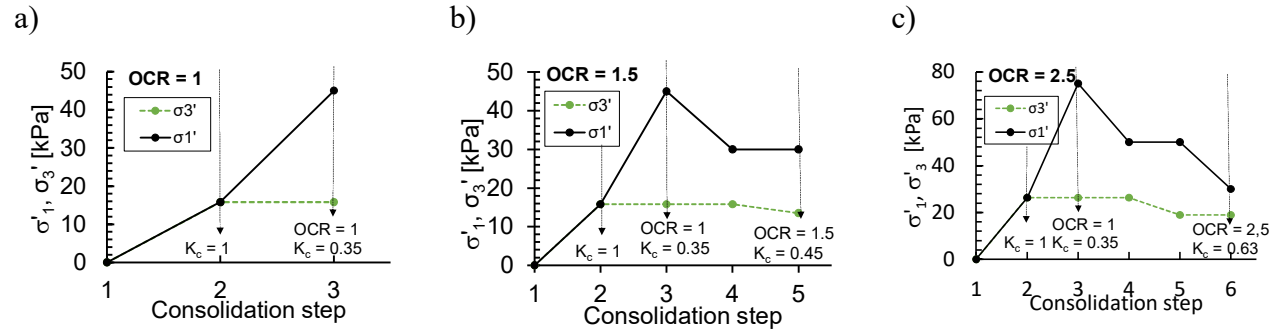

Figure 3. Applied stress paths during the consolidation phase. a) OCR = 1.0, b) OCR = 1.5, and c) OCR = 2.5.

After the consolidation phase, the specimens were sheared undrained at a deformation rate presented in Table 1. The tests were stopped at a maximum axial strain of 25%.

The applied specimen size was a diameter of 63 mm and initial height of 20 mm. Pins with a length of 1.5 mm were used to improve the friction between specimen and plates. The specimens were sheared to a shear strain $\gamma = 40\%$, which was reached after 8 hours for test 66 and 74 and within 4.8 minutes for the rapid tests. The measurement frequency was 0.2 Hz, 1 reading per 5 seconds. The shearing phase of the rapid loading tests contained 58 readings. Further DSS testing details are in accordance with ASTM D6528, [40].

5. Tested material

The peat was sampled by the Deltares Large Diameter Sampler (DLDS) [41], a block sampler that takes samples with a diameter of 0.4 m and a height of 1.0 m. At the laboratory, the different specimens were trimmed from the block sample.

The characteristics of the tested material is given in Table 2, resulting in a volume weight, $\gamma = 10.0$ kN/m^3 with a coefficient of variation, $CoV = 0.06$, and water content, $w = 600$ % with $CoV = 0.05$. For some samples, the volume weight fell below that of water, which could be explained by the presence of gas (see [9,10]).

In Figure 4, we compare the results of the classification tests with the results of earlier tests. The tested specimens in the previous study were retrieved from a slightly shallower depth. The results of both test series were consistent for the volume weight, γ and water content, w. The samples tested in this study had a slightly higher LOI than in the previous study. It should be noted that Figure 4c includes a LOI—value obtained from a spare sample that is not mentioned in Table 2.

Table 2. Characteristics of the tested samples, LOI = loss on ignition, γ = volume weight, and *w* = water content.

Type of test	Depth [m NAP]	LOI [%]	γ [kN/m^3]	*w* [%]
TXL55	−5.01 to −5.15	–	11.8	628.9
TXL56	−4.96 to −5.10	–	10.5	579.4
TXL57	−4.93 to −5.08	83.4	10.2	586.2
TXL58	−4.96 to −5.10	81.8	10.0	607.1
TXL59	−5.01 to −5.15	–	10.2	612.3
TXL60	−5.21 to −5.36	83.5	10.3	639.9
TXL76	−5.19 to −5.33	–	10.1	648.6
TXL77	−5.19 to −5.33	–	10.1	595.2
TXL78	−5.19 to −5.33	–	10.3	645.0
DSS66	−5.10 to −5.12	–	9.7	556.0
DSS67	−5.05 to −5.07	–	9.2	618.1
DSS64	−5.02 to −5.04	–	9.4	552.1
DSS74	−5.00 to −5.02	–	9.3	561.7
DSS75	−4.94 to −4.96	–	9.3	566.8
DSS65	−5.09 to −5.11	–	9.8	594.0

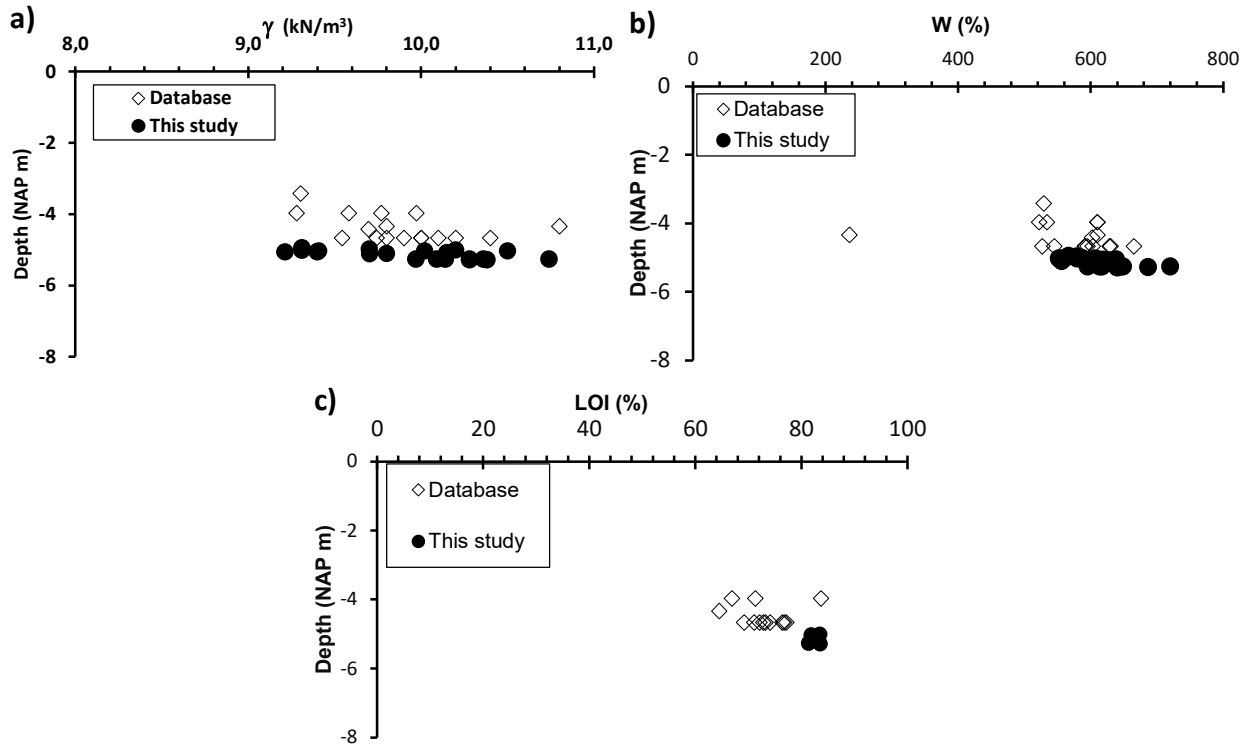

Figure 4. Comparison of sample characteristics to data from database.

Figure 5 shows specimens prior and after triaxial testing. It should be noted that smooth boundary conditions were applied (see section 4), which has a clear impact on triaxial test results on peat [7]. None of the samples failed by a clear failure plane. Instead, different failure mechanisms were observed, mainly containing a wedge failure, in which specimen 55, Figure 5b, showed an asymmetrical mechanism, and specimen 57 showed failure mainly in the lower part of the specimen.

Figures 5c and 5f show the specimen cut in half and provide the opportunity to see the structure of the peat. The presence of wood, the coarse red/orange particles, is visible. The specimens appear to lack the presence of a fine root network, which corresponds to the peat description given in section 3.

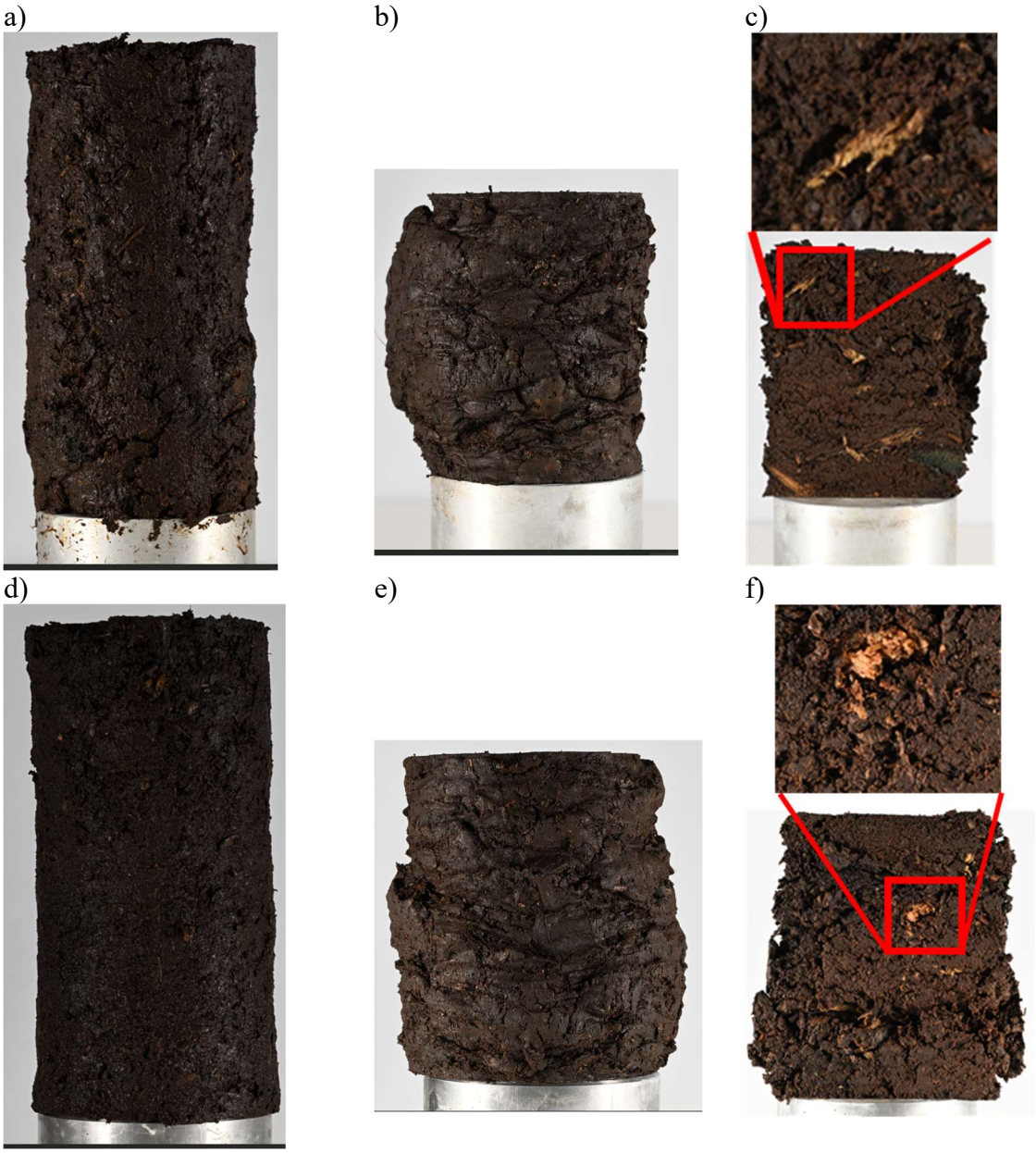

Figure 5. Photos of tested specimens; a) Specimen 55 prior to testing, b) specimen 55 after testing, c) specimen after testing, cut in half, d) specimen 57 prior to testing, e) specimen 57 after testing, and f) specimen 57 after testing, cut in half. c and f provide a close up for further detail.

6. Results of Triaxial testing

To enable comparisons, the stress paths obtained for the triaxial tests were normalised by the isotropic pre-consolidation stress, p'_0, in which p'_0 is the tip of the yield contour reached during the consolidation phase (see definition sketch in Figure 6). The assessment of p'_0 follows from the applied isotropic consolidation stress, p'_c, the deviatoric consolidation stress, q_c, and the mathematical expression for the yield curve [43]:

$$f = q^2 - M^2\left(p'\left(p'_0 - p'\right)\right) = 0 \tag{3}$$

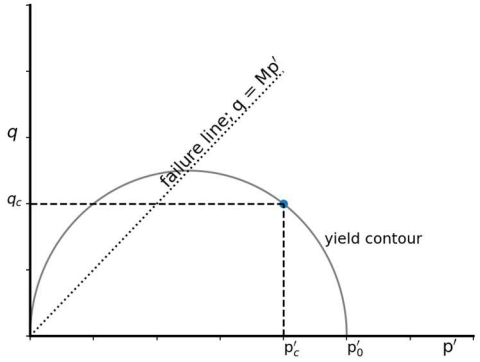

Figure 6. Definition sketch. p'_c and q_c represent the isotropic effective stress and deviatoric stress conditions during consolidation, respectively. p'_0 is the isotropic effective stress at the tip of the corresponding yield curve.

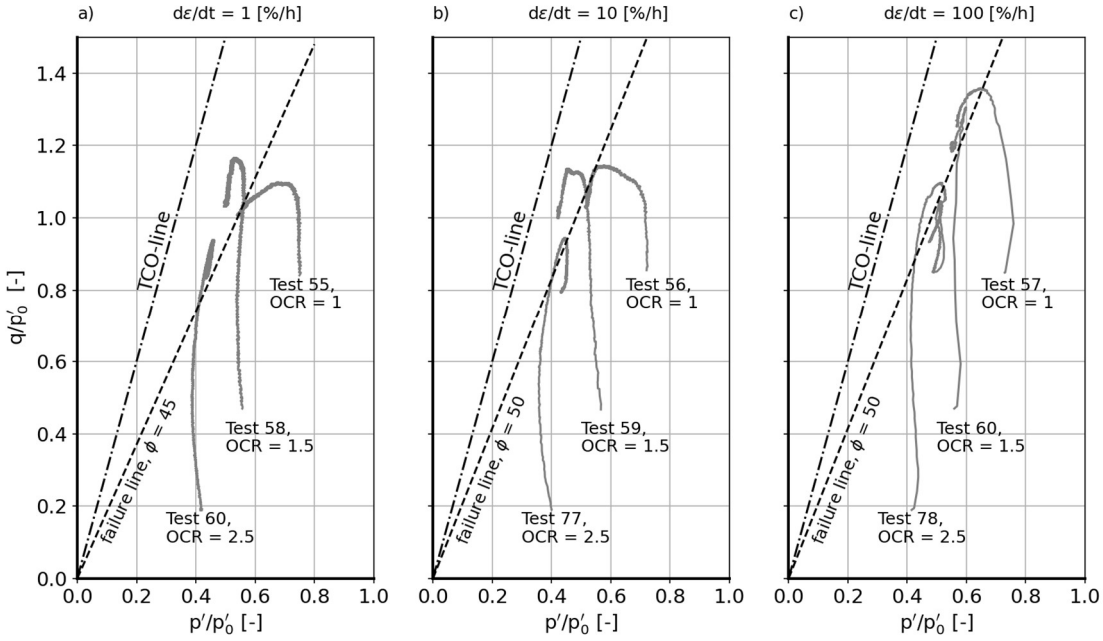

Figure 7. Stress paths normalised for p'_0. a) For strain rate, $d\varepsilon/dt = 1$ %/h, b) $d\varepsilon/dt = 10$ %/h, and c) $d\varepsilon/dt = 100$ %/h. For the definition of p'_0, see Figure 6.

Figure 7 shows the normalised stress paths and the position of the tension cut off (TCO) line. This line represents the conditions for which the minor principal stress is reduced to 0. In contrast to the findings in [3,6,11], the stress paths do not reach the TCO-line, and failure is at a lower strength. This difference in behaviour can be explained by the difference in peat structure. Due to the absence of the fine fibre network, no fibre re-enforcement is active. This results in lower strength than found for tests that include a fine fibre network.

The different tests are expected to fail at the same failure line, with strain rate and OCR having an impact on the exact location at which the stress path hits the failure line [19]. The test results indicate some variation in failure line, as shown in Figure 7. This variation is explained by natural variability.

Figure 8 shows the relation between the normalized failure load, q_f, and the applied axial strain rate, $d\varepsilon_a/dt$. The results are shown for the peak strength and the large strain approach. The large strain, ε_a = 25%, results are used as a proxy for critical state strength [43]. Figure 8 includes fits of the data points, in which the slope of the fitted line represents ρ_q (see equation (1)).

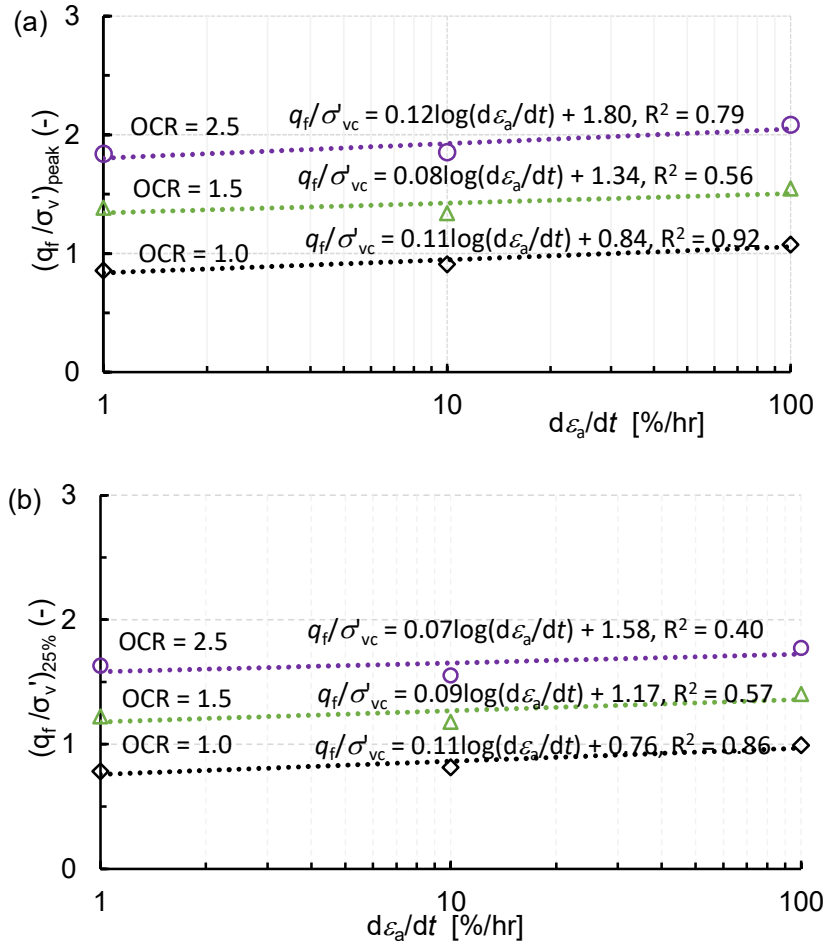

Figure 8. Dimensionless failure load. q_f/σ'_v is a function of the applied strain rate on a semi-logarithmic scale for a) peak strength and b) large strain approach. R^2 = the weighted least square sum.

Following [20] and Equation (1), we used a logarithmic relationship to fit the data in Figure 8. It should be noted that the researchers in [20] discuss isotropic consolidated triaxial test results. The tests discussed in this paper are consolidated anisotropic, and the vertical consolidation stress, σ'_{vc}, is used to normalise the failure load q_f. An impression of the quality of the fit can be obtained from the weighted sum of least squares, R^2, which approaches 1.0 for a perfect fit. The peak strength approach results in better fits with larger R^2 -values than those found for the large strain approach.

Figure 9 shows the same results presented on a linear scale. On a linear scale, the fits have a larger R^2-value than those for the logarithmic scale. This can be explained by the choice of applied strain rates, for which, on a linear scale, the slowest and medium rate are relatively close to each other.

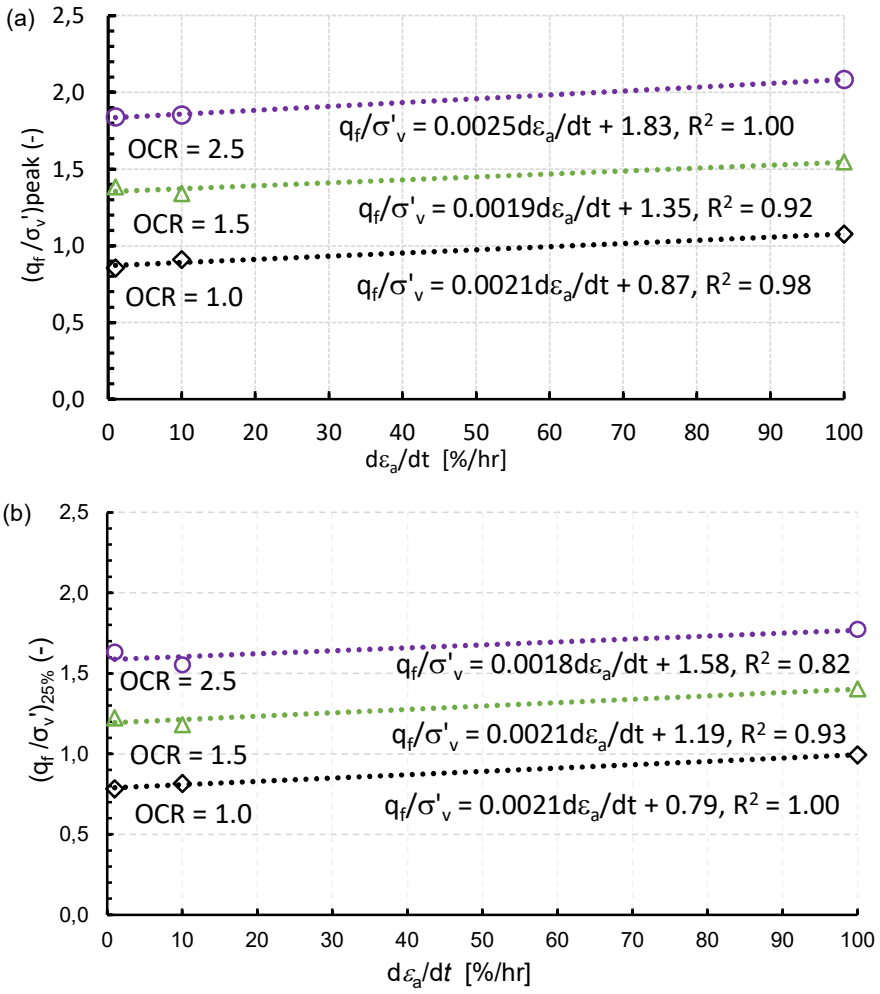

Figure 9. Dimensionless failure load. q_f/σ'_v is a function of the applied strain rate on a linear scale for a) peak strength and b) large strain approach. R^2 = the weighted least square sum.

Figures 8 and 9 lead to the following observations:

- The tests show a positive influence of the applied strain rate on the undrained shear strength; a strain rate increase results in an undrained shear strength increase.

- On a logarithmic scale, according to Equation (1), a variety of slope angles, ρ_q, are found, which do not seem to show a consistent trend.
- There is no consistent trend in the impact of the OCR on the obtained values for ρ_q. This observation deviates from [20], where an increase in ρ_q for increasing OCR is reported for tests on Hong Kong clay.
- On a linear scale, the results are more consistent, with a slope angle of approximately 0.002 for peak strength as well as for the large strain approach.

7. Results for DSS testing

Figure 10 shows the normalised stress paths and the stress-strain curves of the DSS tests. The stress paths are normalised by the consolidation stress (see Table 1). The failure line is given, resulting in $\varphi' = 43.6°$, under the assumption that the DSS stress path reaches the top of the Mohr circle at failure [44]. Following [45], the tension cut-off line for DSS testing is represented by the line $\tau = \sigma'_v$ (this line is also added to Figure 10). Equivalent to the triaxial test data, the stress paths do not reach the TCO-line. The stress-strain curve is corrected for the strain, which is applied in the consolidation phase of pre-sheared specimens, and only the shear strain during accumulated the shearing phase is shown.

Figure 11 shows the normalised failure load as a function of the shearing rate.

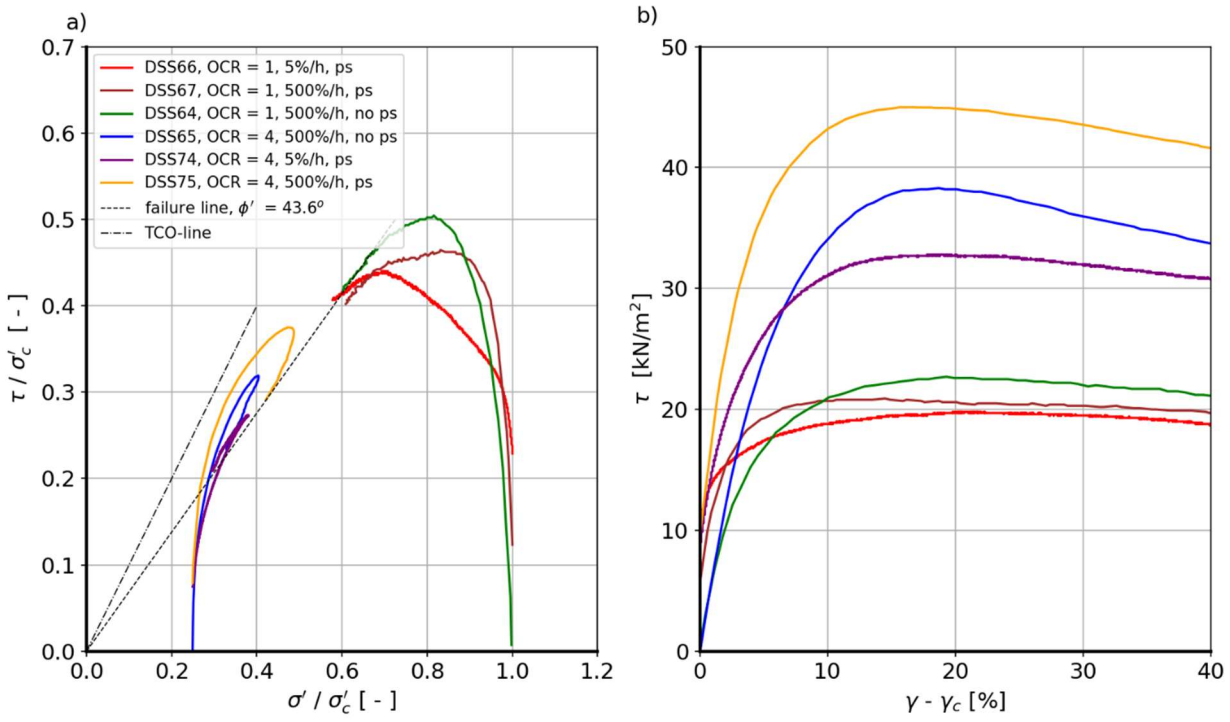

Figure 10. Results of DSS testing. a) Normalised stress paths and b) stress – strain curve. ps = pre-sheared, no ps = not pre-sheared, σ'_c = effective vertical stress during consolidation, and γ_c = shear strain developed by pre-shearing.

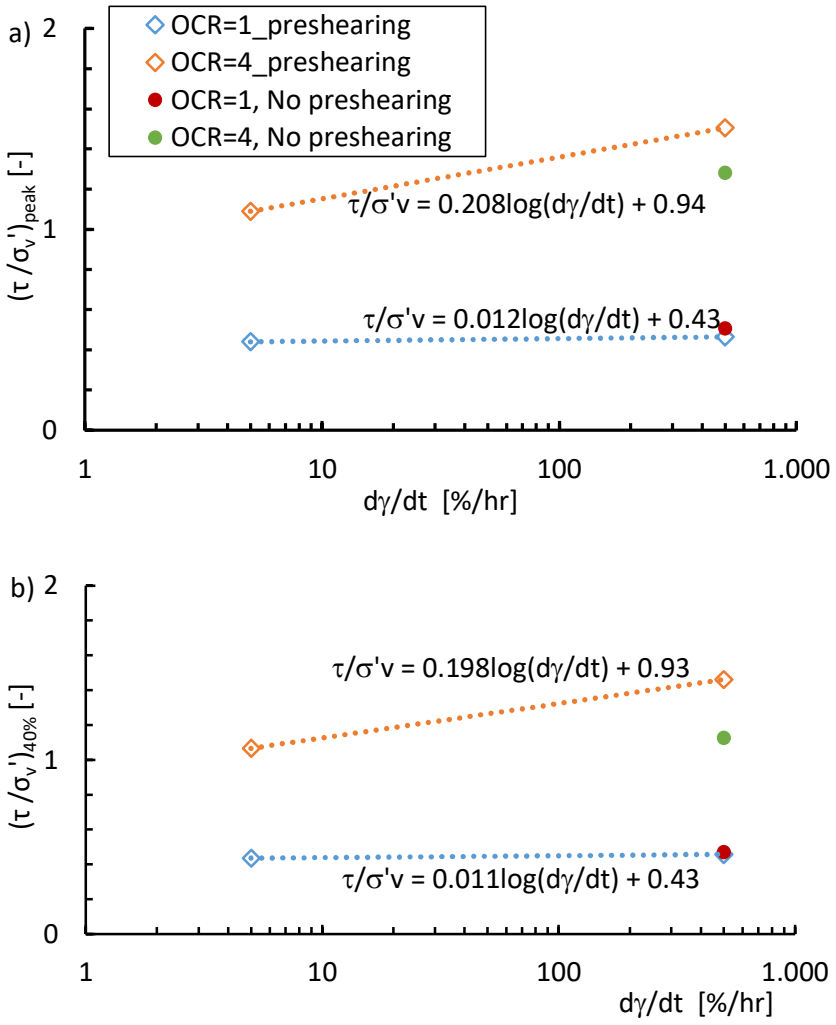

Figure 11. Dimensionless failure load τ/σ'_v, as a function of the applied shear strain rate on a semi-logarithmic scale. a) peak strength and b) large strain strength.

Figures 10 and 11 yield the following observations:

- All stress paths indicate failure at practically the same failure line (see Figure 10a),
- The pre-shearing has a clear impact on the initial part of the stress-strain curve, showing an initial stiff behaviour (see Figure 10b).
- Rate effects are more pronounced for the over consolidated tests, with OCR = 4, than for the normally consolidated tests, OCR = 1.
- For the over-consolidated tests, pre-shearing and increasing strain rate have a favourable impact on the undrained shear strength.
- For the normally consolidated tests, the strengths differ slightly. In contrast to the over-consolidated tests, the rapid pre-sheared test reaches approximately the same strength as the rapid non-pre-sheared test. This difference in behaviour might be explained by heterogeneity (see discussion in Section 9).
- Since only two strain rates are tested for the DSS tests, a perfect fit is seen in Figure 11, and additional fitting on a normal scale does not provide additional information.

- The impact of OCR on the test results is also visible in Figure 11. In contrast to the triaxial test results, the impact of strain rate for normally consolidated conditions is almost absent, and the relation failure load vs strain rate runs almost horizontal. This might be explained by the natural variability between the samples, as discussed in Section 9.

8. Numerical simulations

Simulations of the triaxial test data were conducted using the Creep-SClay1 model [15,46]. We used the implementation of the model, described in [47], in combination with the soil test module in PLAXIS 2D 2024 [48]. The Creep-SClay1 model is a cam-clay type model that enables rotation of the yield curve induced by a plastic strain conform [49–51] and includes a creep formulation conform [52], which is based on the isotach concept [16,17].

Grimstad et al. [14] and Sivasithamparam et al. [15] showed the applicability of the model to simulate strain rate effects in triaxial testing of clays. In this section, we investigate the applicability of this model to simulate peat behaviour.

Simulation of the results was done in two steps. First, curve fitting of the triaxial test TX55, OCR = 1 and $d\varepsilon_a/dt$ = 1%/hour, provided the parameter set. Second, the derived parameter set was used to simulate the other tests. Table 3 shows the applied parameters.

Table 3. Model parameters.

parameter	symbol	unit	value
Re-compression index	κ^*	[–]	0.025
Compression index	λ^*	[–]	0.25
Creep parameter	μ^*	[–]	8.252×10^{-3}
Poisson's rate	ν	[–]	0.15[a]
Friction angle[b]	φ'	[°]	45–50[c]
Rotational hardening parameter	ω	[–]	0
Rotational hardening parameter	ω_d	[–]	0
Reference time for creep	τ_0	[day]	1[a]
Initial yield curve rotation	α_0	[–]	0.358

[a] default value

[b] the used implementation enables a difference in friction angle for compression, φ'_c, and extension, φ'_e; here, $\varphi'_c = \varphi'_e$.

[c] applied values according to values presented in Figure 7

In Table 3, the initial yield curve rotation, α_0, was derived according to [49]:

$$\alpha_0 = \alpha_{K_0} = \frac{\eta_{K_0}^2 + 3\eta_{K_0} - M^2}{3}; \quad \eta_{K_0} = \frac{3\left(1 - K_{0,NC}\right)}{1 + 2K_{0,NC}} \tag{4}$$

where α_{Ko} represents the yield curve rotation under $K_{0,NC}$ loading conditions and M the slope of the failure line (see Figure 6) in triaxial compression. The justification in applying α_{Ko} in all tests is that

all triaxial tests were pre-consolidated at $K_{0,NC}$ conditions. The Creep SClay1 model accounts only for yield curve rotation under yielding conditions, and the yield curve remains fixed at unloading when no plastic strains are developed. Consequently, the consolidation paths depicted in Figure 3 will first rotate the yield curve to α_{Ko}, and at unloading, the yield curve will remain in this rotated position.

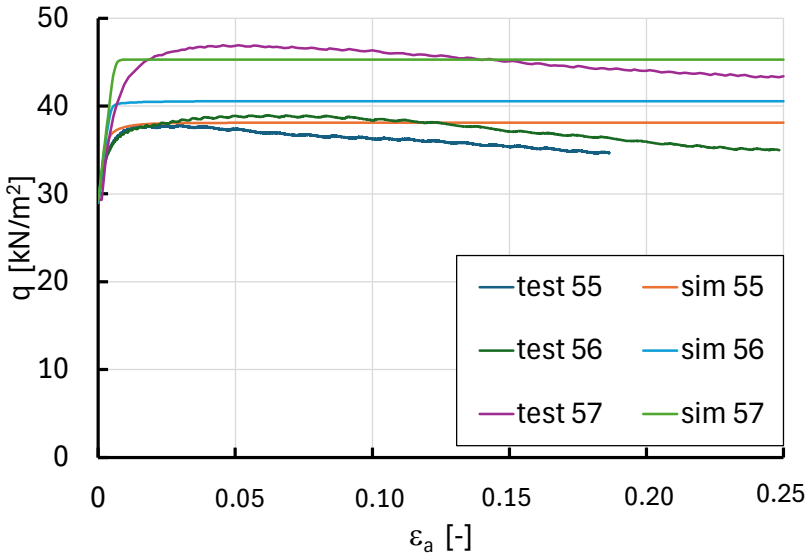

Figure 12. Comparison of test results and simulations for OCR = 1.0, φ'= 45°, Test TX55 with dε/dt = 1 %/h, Test TX56 with dε/dt 10 %/h, and Test TX57 with dε/dt 100 %/h.

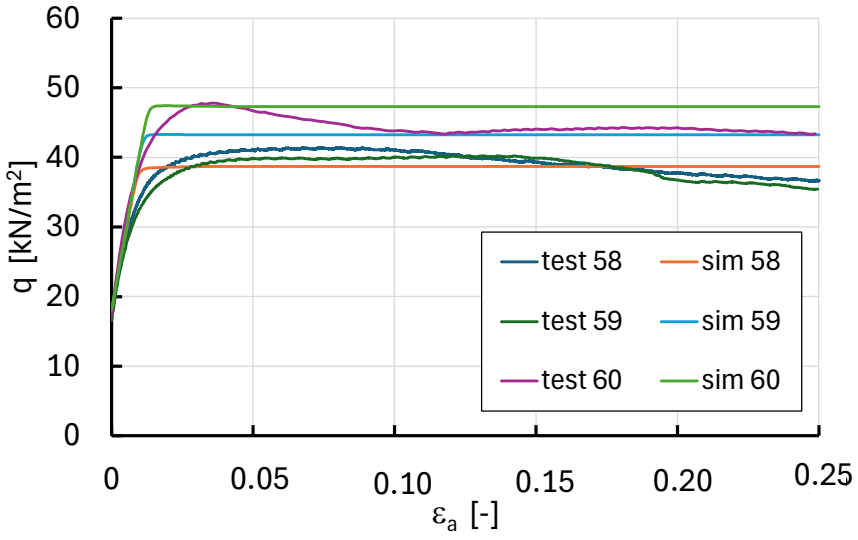

Figure 13. Comparison of test results and simulations for OCR = 1.5, φ'= 50°, Test TX68 with dε/dt = 1 %/h, Test TX59 with dε/dt = 10 %/h, and Test TX60 with dε/dt = 100 %/h.

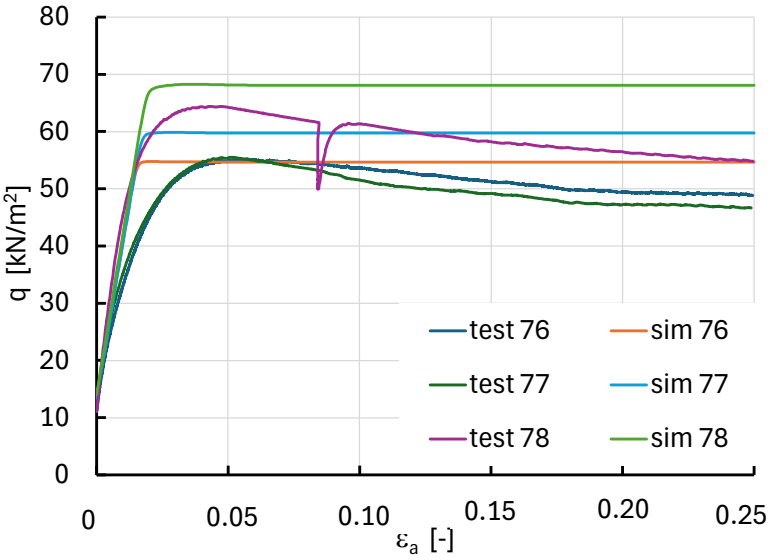

Figure 14. Comparison of test results and simulations for OCR = 2.5, φ'= 50° Test TX76 with dε/dt = 1 %/h, Test TX77 with dε/dt = 10 %/h, and Test TX78 with dε/dt = 100 %/h.

The simulations did not include rotation of the yield curve except from the initial rotation, α_0, and the corresponding rotational hardening parameters, ω and ω_d, set to 0.

Figures 12, 13, and 14 provide the comparison between measurements and simulations. Figure 7 shows the variability in friction angle, in which the tests with OCR = 1.0 yield φ'= 45°, while φ'= 50° is found for the other tests. This variation is also applied to the simulations.

The numerical simulations are in reasonable agreement with the test data for dε/dt = 1 %/h and 100 %/h. However, there is a mismatch for the simulations for the tests with dε/dt = 10 %/h. For the three tested values of OCR, the differences in the test result for dε/dt = 1%/h and 10%/h seems small, and is smaller than predicted by the numerical simulations.

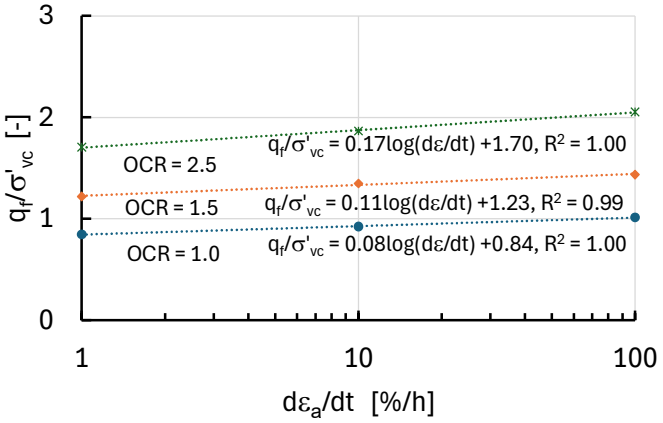

Figure 15. Dimensionless failure load, q_f/σ'_{vc}, as a function of the applied strain rate for the numerical simulations.

Figure 15 shows Equation (1) for the numerical analysis. The numerical simulations comply to the trend reported in [20] for Hong Kong clay; the increase in dimensionless failure load, q_f/σ'_{vc}, is linear on a logarithmic scale, and ρ_q increases with increasing OCR.

9. Discussion

In contrast to the numerical simulations, the differences in test results for triaxial tests conducted at $d\varepsilon/dt$ = 1 %/h and the results for tests run at $d\varepsilon/dt$ = 10 %/h are small to negligible, as shown in Figures 12 to 14. This can be explained by the natural heterogeneity of the tested material. Figure 7 indicates that the friction angle of the tested material ranges between 45° and 50°. Figure 16 provides the results of a further analysis of test TX76 with OCR = 2.5 and $d\varepsilon_a/dt$ = 1 %/h and test TX77 with OCR = 2.5 and $d\varepsilon_a/dt$ = 10 %/h. The test data is compared to the simulations of test TX77 with φ' = 45° and TX76 with φ' = 50°, while keeping other parameters equal to those in Table 3. The simulations show that the variation of φ' counter act to variation in strain rate, and little difference is found in the stress-strain curves. This illustrates the impact of heterogeneity on the test results, in which the difference in test results for tests conducted for a strain rate of $d\varepsilon_a/dt$ = 1 %/h and $d\varepsilon_a/dt$ = 10 %/h are masked by heterogeneity.

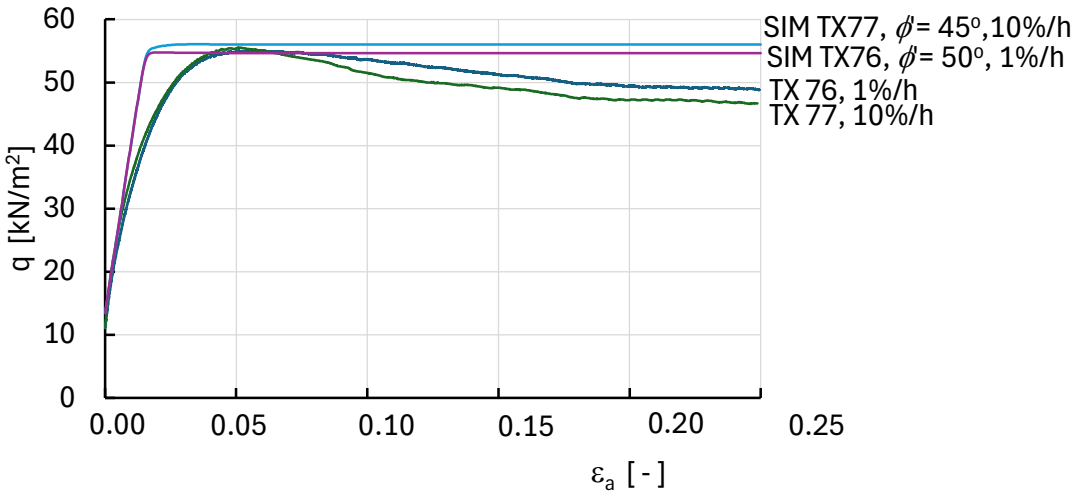

Figure 16. Simulation of test TX76 and TX77 with variation in φ', OCR = 2.5.

The difference in test results between $d\varepsilon_a/dt$ = 1 %/h and $d\varepsilon_a/dt$ = 100 %/h are more pronounced than the differences between $d\varepsilon_a/dt$ = 1 %/h and $d\varepsilon_a/dt$ = 10 %/h and are therefore not masked by heterogeneity.

The results for tests TX76 and TX77 are shown here as an example, and equivalent results are found for the simulations of tests TX58, $d\varepsilon_a/dt$ = 1 %/h, and TX59, $d\varepsilon_a/dt$ = 10 %/h, both at OCR = 1.5, and tests TX55, $d\varepsilon_a/dt$ = 1 %/h, and TX56, $d\varepsilon_a/dt$ = 10 %/h, both at OCR = 1.0.

Moreover, the DSS test results can be better understood when considering the natural variability. The tests for OCR = 1.0 in Figure 11 combine the DSS test with the highest water content, DSS67, and

the DSS test with the lowest water content, DSS66 (Table 2). This variability veils the expected strength increase due to the strain rate increase.

The values for ρ_q obtained for peats range between 0.07–0.12 (see Figure 8). These values are larger than the values reported in [20] for Hong Kong clay, $\rho_q = 0.014$ for OCR = 1 and $\rho_q = 0.034$ for OCR = 2. The observation that peat strength has a stronger strain rate dependency than for clays can be related to the larger susceptibility for creep that peats typically show [8,9].

10. Conclusions

The triaxial tests and the DSS tests show the strain rate dependency of the undrained shear strength of peat. The general trend, where more strength is found for higher strain rates, complies with the general trend for clays. The trend, expressed by ρ_q, found in this paper is larger than the values reported for clays [20].

Due to the heterogeneity of the tested specimen, which is typical for peats, more detailed trends are difficult to establish. For a strain rate increase from $d\varepsilon_a/dt$ = 1%/h to $d\varepsilon_a/dt$ = 10%/h, the positive effect of strain rate increase is masked by the variability of peat characteristics. For a strain rate increase from $d\varepsilon_a/dt$ = 1%/h to $d\varepsilon_a/dt$ = 100%/h, the effect of strain rate increase extends beyond the effect heterogeneity.

The over-consolidated DSS tests show an influence of OCR on strain-rate dependency, which is not clearly found in the triaxial tests.

Visual observations show that the fibrosity and corresponding tensile strength is low for the tested peat. This impacts the failure paths found in the triaxial tests, which, in contrast to some literature data, does not reach the TCO-line.

When considering the observed heterogeneity, the Creep SClay1 model produces a reasonable simulation of the peak strengths found in the tests.

The tests provide a starting point for exploring rate effects in testing peats. Additional tests and numerical simulations by different constitutive models that account for viscous effects are suggested to further our understanding of peat behaviour.

Author contributions

Cor Zwanenburg: writing–original draft, writing–review & editing, Conceptualization, Formal analysis, Visualization. Maria Konstadinou: writing–review & editing, Investigation, Visualization. Edward Grünewald: writing–review & editing, Resources; Funding acquisition.

Use of AI tools declaration

The authors declare they have not used Artificial Intelligence (AI) tools in the creation of this article.

Acknowledgements

The authors would like to thank ProRail and the research programme RESET for financially supporting this research.

Conflict of interest

The authors declare no conflict of interest.

References

1. Hobbs NB (1986) Mire morphology and the properties and behaviour of some British and foreign peats. *Q J Eng Geol Hydrogeol* 19: 7–80. https://doi.org/10.1144/GSL.QJEG.1986.019.01.02
2. Landva AO (2007) Characterization of Escuminac peat and construction on peatland, In: Tan TW, Phoon KK, Hight DW, et al. Eds., *Characterisation and Engineering Properties of Natural Soils,* London, UK: Taylor and Francis Group.
3. Yamaguchi H, Ohira Y, Kogure K, et al. (1985) Undrained shear characteristics of normally consolidated peat under triaxial compression and extension conditions. *Soils Found* 25: 1–18. https://doi.org/10.3208/sandf1972.25.3_1
4. Cola S, Cortelazzo G (2005) The shear strength behavior of two peaty soils. *Geotch Geol Eng* 23: 679–695. https://doi.org/10.1007/s10706-004-9223-9
5. Hendry MT, Sharma JS, Martin CD, et al. (2012) Effect of fibre content and structure on anisotropic elastic stiffness and shear strength of peat. *Can Geotech J* 49: 403–415. https://doi.org/10.1139/T2012-003
6. O'Kelly BC (2017) Measurement, interpretation and recommended use of laboratory strength properties of fibrous peat. *Geotech Res* 4: 136–171. http://dx.doi.org/10.1680/jgere.17.00006
7. Jommi C, Chao CY, Muraro S, et al. (2021) Developing a constitutive approach for peats from laboratory data. *Geomech Energy Environ* 27. https://doi.org/10.1016/j.gete.2020.100220
8. Mesri G, Ajlouni M (2007) Engineering Properties of Fibrous Peats. *J Geotech Geoenviron Eng* 133: 850–866. https://doi.org/10.1061/(ASCE)1090-0241(2007)133:7(850)
9. Den Haan EJ, Kruse G AM (2006) Characterisation and engineering properties of Dutch peats. *Characterisation and Engineering of Natural Soils*, Singapore, London, UK: Taylor and Francis. 3: 2101–2133.
10. Zwanenburg C, Den Haan EJ, Kruse GAM, et al. (2012) Failure of a trial embankment on peat in Booneschans, the Netherlands. *Géotechnique* 62: 479–490. http://dx.doi.org/10.1680/geot.9.P.094
11. Zwanenburg C, Jardine RJ (2015) Laboratory, in situ and full-scale load tests to assess flood embankment stability on peat. *Géotechnique* 65: 309–326. http://dx.doi.org/10.1680/geot.14.P.257
12. Muraro S (2019) *The deviatoric behaviour of peat: a route between past empiricism and future perspectives*. PhD Thesis, Delft University of Technology, the Netherlands. https://doi.org/10.4233/uuid:ffbea4e0-2e97-4d41-819d-beec42120b29

13. Lengkeek HJ (2022) *Testing and modelling of sheet pile reinforced dikes on organic soils; Insights from the Eemdijk full-scale failure test*. PhD Thesis, Delft University of Technology, the Netherlands. https://doi.org/10.4233/uuid:78df5e2b-740e-4268-a821-ed0ccaae93e5
14. Grimstad G, Degago S, Nordal S, et al. (2010) Modelling creep and rate effects in structured anisotropic soft clays. *Acta Geotech* 5: 69–81. https://doi.org/10.1007/s11440-010-0119-y
15. Sivasithamparam N, Karstunen M, Bonnier P (2015) Modelling creep behaviour of anisotropic soft soils. *Comput Geotech* 69: 46–57. https://doi.org/10.1016/j.compgeo.2015.04.015
16. Šuklje L (1957) The analysis of the consolidation process by the isotache method. *Proceedings of the 4th international conference on soil mechanics and foundation engineering*, London, 1: 200–206.
17. Leroueil S (2006) The isotache approach. Where are we 50 years after its development by Professor Suklje? Prof. Suklje's memorial lecture, *Proceedings of the 13th Danube-European Conference on Geotechnical Engineering,* Ljubljana, Slovenia, 55–88.
18. Casagrande A, Wilson SD (1951) Effect of rate of loading on the strength of clays and shales at constant water content. *Géotechnique* 2: 251–263. https://doi.org/10.1680/geot.1951.2.3.251
19. Vaid YP, Campanella RG (1977) Time-dependent behavior of undisturbed clay. *J Geotech Eng Div* 103: 693–709. https://doi.org/10.1061/AJGEB6.0000449
20. Zhu JG, Yin JH (2000) Strain-rate-dependent stress-strain behavior of overconsolidated Hong Kong marine clay. *Can Geotech J* 37: 1272–1282. https://doi.org/10.1139/t00-054
21. Han J, Dano C, Hicher PY, et al. (2014) Strain-rate dependency of shear strength for a highly overconsolidated clay, *Soil Behavior and Geomechanics*, 343–352. https://doi.org/10.1061/9780784413388.035
22. Wang H, Cui YJ, Vu MN, et al. (2024) Strain-rate effect on the hydro-mechanical behaviour of unsaturated damaged Callovo-Oxfordian claystone. *Acta Geotech* 19: 4313–4324 https://doi.org/10.1007/s11440-023-02143-5
23. Bjerrum L, Aitchison GD (1973) Problems of soils mechanics and construction on soft clays and structurally unstable soils (collapsible, expensive and others). *8th International Conference on Soil Mechanics and Foundation Engineering (Moscow)*, 2: 109–159.
24. Lunne T, Robertson PK, Powell JJM (1997) Cone Penetration Testing in geotechnical practice. Blackie Academic & Profesional, London.
25. Dejong J, Yafrate N, DeGroot D, et al. (2010) Recommended practice for full-flow penetrometer testing and analysis. *Geotech Test J* 33: 137–149. https://doi.org/10.1520/GTJ102468
26. Tatsuoka F, Ishihara M, Di Benedetto H, et al. (2002) Time-dependent shear deformation characteristics of geomaterials and their simulation. *Soils Found* 42: 103–129. https://doi.org/10.3208/sandf.42.2_103
27. Länsivaara T (1999) *A study of the mechanical behavior of soft clay*. PhD Dissertation, Norwegian University of Science and Technology (NTNU).
28. Wang H, Cui YJ (2023) A viscoplastic constitutive model for unsaturated soils based on nonstationary flow surface theory. *Int J Numer Anal Methods Geomech* 48: 476–495. https://doi.org/10.1002/nag.3648

29. Bjerrum L (1967) Engineering geology of Norwegian normally-consolidated marine clays as related to settlements of buildings. *Géotechnique* 17: 81–118. https://doi.org/10.1680/geot.1967.17.2.83
30. KTC Zegveld, Dutch, 2025. Available from: https://www.ktczegveld.nl/.
31. Massop HTL, Hessel R, van den Akker JJH, et al. (2024) Monitoring long-term peat subsidence with subsidence platens in Zegveld, the Netherlands. *Geoderma* 450. https://doi.org/10.1016/j.geoderma.2024.117039
32. Zwanenburg C, Wittekoek B, Konstadinou M (2024) Creep of organic soils due to small load increments, *Geotechnical Engineering Challenges to Meet Current and Emerging Needs of Society,* CRC Press.
33. AHN, Algemene Hoogtekaart Nederland (height map of the Netherlands), 2025. Available from: https://www.ahn.nl/ahn-viewer.
34. Schothorst CJ (1977) Subsidence of low moor peat soils in the western Netherlands. *Geoderma* 17: 265–291. https://doi.org/10.1016/0016-7061(77)90089-1
35. TAW, Technisch rapport 16; geotechnische classificatie van veen. Technische Advies commissie voor de Waterkeringen Delft. In: Dutch. 1996. Available from: https://open.rijkswaterstaat.nl/@227322/technisch-rapport-geotechnische/.
36. Erkens G, de Vries S, Zwanenburg C, et al. (2013) Dijken op veen II, veenbeschrijvingsprotocol. Deltares report nr 1208254-013. In Dutch.
37. NNI-ISO, Geotechnical investigation and testing—laboratory testing of soils—Part 9: consolidated triaxial compression tests on water saturated soils. NEN-EN-ISO 17892-9. Nederlands Normalisatie instituut, NNI, Delft, the Netherlands. 2018. Available from: https://www.nen.nl/nen-en-iso-17892-9-2018-en-245588.
38. Konstadinou M, Zwanenburg C (2020) A critical review of membrane and filter paper correction formulas for the triaxial testing of soft soils. *Geotech Test J* 43: 1–19. https://doi.org/10.1520/GTJ20180047
39. Dyvik R, Berre T, Lacasse S, et al. (1987) Comparison of truly undrained and constant volume direct simple shear tests. *Géotechnique* 37: 3–10. https://doi.org/10.1680/geot.1987.37.1.3
40. ASTM, Standard Test Method for Consolidated Undrained Direct Simple Shear Testing of Fine Grains soils. ASTM D6528. West Conshohocken, PA: ASTM. 2017.
41. Zwanenburg C (2017) The development of a large diameter sampler. 19th ICSMGE, Seoul, Korea.
42. Wood DM (1990) *Soil behaviour and critical state soil mechanics*, Cambridge, UK: Cambridge University Press.
43. Leroueil S, Magnan JP, Tavenas F (1990) *Embankments on soft clays*, Ellis Horwood.
44. DeGroot DJ, Ladd CC, Germaine JT (1992) *Direct simple shear testing of cohesive soils*, Constructed Facilities Division, Department of Civil Engineering, Massachusetts Institute of Technology.
45. Den Haan EJ (2014) Modelling peat with an anisotropic time-dependent model for clay, In: Hicks MA, Brinkgreve RBJ, Rohe A, Eds., *Numerical methods in geotechnical engineering*, London: Taylor & Francis Group, 55–60.

46. Sivasithamparam N, Karstunen M, Brinkgreve R, et al. (2013) Comparison of two anisotropic creep models at element level. *International Conference on Installation Effects in Geotechnical Engineering*, 18.
47. Zwanenburg C, Aboufirass A, Teunissen JAM (2018) POVM Validatie uitgangspunten en lange termijn ontwikkeling, Deltares report nr 11200999-002-001. In Dutch. Available from: https://publicwiki.deltares.nl/spaces/HWBPMacro/pages/347997328/Achtergronddocumenten+en+Software+POVM+Archief?preview=/347997328/347997344/Deltares-11200999-002-GEO-001-POVM-Creep-SClay1-Final2-secr.pdf.
48. Bentley, Manual PLAXIS 2D 2024.3, 2024. Available from: https://bentleysystems.service-now.com/community?id=kb_article&sysparm_article=KB0107989.
49. Wheeler SJ, Näätänen A, Karstunen M, et al. (2003) An anisotropic elastoplastic model for soft clays. *Can Geotech J* 40: 403–418. https://doi.org/10.1139/T02-119
50. Dafalias YF, Taiebat M (2013) Anatomy of rotational hardening in clay plasticity. *Géotechnique* 63: 1406–1418. https://doi.org/10.1680/geot.12.P.197
51. Dafalias YF, Taiebat M (2014) Rotational hardening with and without anisotropic fabric at critical state. *Géotechnique* 64: 507–511. https://doi.org/10.1680/geot.13.T.035
52. Vermeer PA, Neher HP (1999) A soft soil model that accounts for creep. *Beyond 2000 in computational geotechnics,* Balkema, Rotterdam, 249–261.

AIMS Press

© 2025 the Author(s), licensee AIMS Press. This is an open access article distributed under the terms of the Creative Commons Attribution License (https://creativecommons.org/licenses/by/4.0)